



4

Mass-selected ion spectroscopy of K-shell excited polyatomic molecules: Fragmentation competing with intramolecular energy relaxation

Toshio Ibuki¹ and Kazumasa Okada²

¹Kyoto University of Education, Fushimi-ku, Kyoto 612-8522, Japan; ²Department of Chemistry, Hiroshima University, Higashi-Hiroshima 739-8526, Japan

1. Introduction

Synchrotron radiation has greatly progressed in these two decades as a soft X-ray light source for studying inner shell photochemistry of atoms and molecules. One of the great progresses in the soft X-ray photochemistry is the reaction dynamics of K-shell excited molecules. The angular distribution of fragment ions ($d\sigma/d\Omega$) produced after core excitation with linearly polarized soft X-ray is expressed by the following simple expression within the axial recoil approximation [1-3]:

$$d\sigma/d\Omega = (\sigma_i/4\pi)[1 + \beta P_2(\cos\theta)] \quad (1)$$

where σ is the absorption cross section, Ω is the solid angle, σ_i is the total photoabsorption cross section over space, $P_2 = (3\cos^2\theta - 1)/2$, which is the Legendre polynomial of degree two, θ is the angle between the

direction of light polarization and the internuclear axis and β is the anisotropy parameter. In K-shell excited diatomic molecules of N_2 [4-6], O_2 [5-7], NO [8, 9] and CO [6, 9, 10], the fragment ions produced via $\Delta\Lambda = 0$ transitions, such as the $1s \rightarrow \sigma^*$ excitation, are ejected into the direction parallel (0°) to the electric vector of the exciting photon beam. In this case the anisotropy parameter is $\beta = 2$ for a pure $\Sigma_g - \Sigma_u$ transition. In the $\Delta\Lambda = \pm 1$ transition such as the $1s \rightarrow \pi^*$ excitation the fragment ions are detected in the perpendicular direction (90°) and then $\beta = -1$ for a pure $\Sigma - \Pi$ transition. The usefulness of the concept in Eq. (1), which succeeded in understanding the reaction dynamics of diatomic molecules, has been extensively applied in both assigning photoabsorption peaks and elucidating breakdown pathways of the K-shell excited triatomic molecules: N_2O [11,12], CO_2 [13-15], CS_2 , OCS [14] and H_2O [16,17]. However, the analysis is not simple since the Renner-Teller effect comes in the angular distribution of fragment ions emitted from the core excited N_2O and CO_2 molecules [11, 12, 14, 15]. The axial recoil approximation was valid only for the angular distribution of H^+ formed from the O K-shell excited H_2O [16]. The situation gets more complex in a large molecule since an energetic fragment ion should be mass-selected.

Another topic of the inner shell excitation is the site-specific photofragmentation of a polyatomic molecule. Direct ionization of the K-shell electron in a molecule composed of light atoms such as C, N and O usually leads to double electron ejection via normal Auger decay. Thus, the molecule has two positive holes in the valence orbital(s). The mode of excitation of a core electron into a vacant molecular orbital is called the resonant Auger process. If the core electron initially excited to the vacant molecular orbital does not take part in the following Auger decay, one electron in the valence orbitals fills the core hole and another valence electron is released as an Auger electron. The final states of this mode are referred to as two-hole one-particle states, being called spectator Auger decay. If the electron initially excited to the vacant molecular orbital participates in the Auger decay, the molecules are populated in different electronic states with +1 charge, being called the participant Auger process. Sometime the Auger decays are followed by cascading Auger electron emission to produce multiply charged molecular ions, which decompose into fragment ions through Coulomb explosion. The lifetime of core hole excited molecule is usually in the order 10^{-15} s which is shorter than the periods of molecular vibration and rotation with $\approx 10^{-13}$ s, and hence nonstatistical or site-dependent bond dissociation is expected. Such evidences for site-specific soft X-ray photochemistry of molecules have been performed for N_2O [18, 19], O_3 [20], CF_2CH_2 [21], CF_3CH_3 [21, 22], $(CH_3)_2CO$ [18], $Pb(CH_3)_4$ [23], chlorofluorocarbons [24-26], *n*- and 2-propanol [27], and other organic molecules [28-30] by exciting the innermost 1s electron of a specific atom in the molecule. These studies have been done with the expectation that a bond dissociation occurs in a limited area around the specific atom initially excited.

In this paper we report the angle-resolved photofragmentation of K-shell excited polyatomic molecules with pseudo-linear skeleton in the ground state: CF_3CN , CF_3CCH and CF_2CH_2 . Fluorine atom is most electronegative and thus a large chemical shift is induced around the F atom in these compounds. The chemical shift makes it possible to selectively excite the C1s electron of the CF_n ($n = 2$ or 3) group. Site-dependent photofragmentation of non-linear polyatomic molecules will be also studied by changing the molecular length in a series of $CH_3CO(CH_2)_nCN$ ($n = 0-3$). We will focus the discussion on the bond dissociation competing with intramolecular energy relaxation.

2. Experimental

Synchrotron radiation from the UVSOR facility at the Institute for Molecular Science was dispersed using a constant-deviation grazing incidence monochromator, in which three gratings with different grooves were installed to obtain 30-600 eV photons. Typical energy resolution was $E/\Delta E = 2000 - 4000$ for photoabsorption [31]. An aluminum thin filter was used in order to reduce the scattered stray light. The dispersed soft X-ray flux was monitored by a silicon photodiode and recorded simultaneously as the photocurrent. All the spectra were normalized by the photocurrent in order to correct for fluctuations in the dispersed photon flux. The photon energies were calibrated using the π^* resonant transitions of CO at 287.40 eV and N₂ at 401.10 eV [32].

The total photoabsorption cross sections were obtained by using a Samson type double ion chamber [33] with the Al thin filter at the front and the photodiode at the end to monitor the transmitted light intensity. The length of a cathode plate to collect photoions was 10.0 cm and typical gas pressure was 30 Pa. Lambert-Beer law was assumed.

The main chamber equipped with a time-of-flight (TOF) mass spectrometer was rotatable from a -20 to 110° angle with respect to the linear electric vector of the synchrotron radiation beam. The TOF mass spectra were acquired by means of a total photoelectron-photoion coincidence method. The TOF mass spectrometer was used in two modes: One was as a linear TOF (L-TOF) spectrometer operated under Wiley-McLaren space focusing conditions [34]. In this L-TOF measurement a low electrostatic field of -250 V/cm was supplied to extract the fragment ions. Another is a reflectron type time-of-flight (R-TOF) mass spectrometer to achieve a high mass resolution $M/\Delta M \geq 100$ even for fragment ions with kinetic energies up to ≈ 10 eV [29, 35]. In the R-TOF mode, high potentials of ± 1500 V/cm were supplied across the ionization region to collect the ions formed. Two lens systems were installed in the flight tube in order to focus the fragment ions on the ion detector. Commercial gas samples of CF₃CN, CF₃CCH and CF₂CH₂ were used without further purification. The samples of CH₃COCN and CH₃CO(CH₂)₃CN supplied commercially were used after distillation in a vacuum to collect the middle fraction. The samples of CH₃COCH₂CN and CH₃CO(CH₂)₂CN were synthesized according to the procedures published [36, 37]. These synthesized samples were also distilled in a vacuum before use. The sample was introduced in the main chamber as an effusive jet.

3. Angle-resolved, mass-selected ion spectroscopy of K-shell excited CF₃CN and CF₃CCH

The CF₃CN and CF₃CCH molecules have the pseudo-linear skeletons in the ground states. Thus, excitation of the K-shell electron of these molecules by using linearly polarized soft X-rays would be a test case to examine the applicability of Eq. (1) to polyatomic molecules. These molecules give us fruitful information for starting the studies on reaction dynamics of the inner shell excited polyatomic molecules.

3.1. CF₃CN excited at the N and C K-shell electrons

3.1.1. Photoabsorption spectra

The top panel of Fig. 1 shows the total photoabsorption cross section of CF₃CN in the C K-shell region [38]. The open circles are the experimental data. The humps around

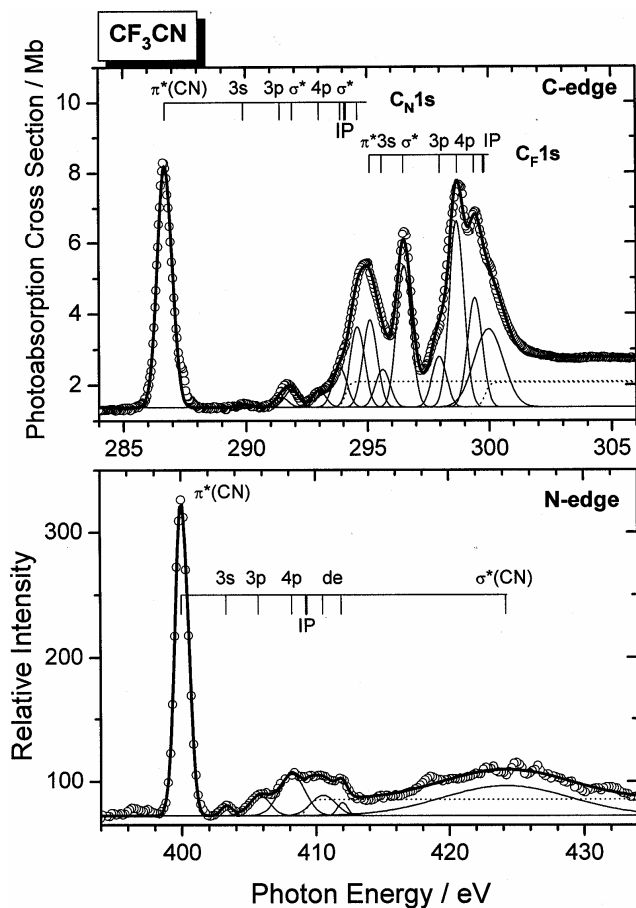


Figure 1. Photoabsorption spectra of CF_3CN at the C K-shell (top panel) and N K-regions (bottom panel). The open circles are the experimental data. The solid curves were obtained by a least-squares curve fitting with Gaussian functions. Peak positions are shown by bars. The “de” means double excitation. The details are given in Refs. 38 and 40.

295 and 299 eV are overlapped by some electronically excited states. In order to estimate the embedded peak positions, we carried out a least-squares curve fitting with Gaussian functions. The thin solid curves are the electronic transitions obtained by the least-squares curve fitting. The thick curve is the sum of the thin ones. The details of the peak assignments were discussed on the basis of the term values and quantum defects in the previous paper [38]. Briefly, the distinct peaks at 286.7 and 296.5 eV are assigned to the $\text{C}_\text{N}1s \rightarrow \pi^*(\text{CN})$ and $\text{C}_\text{F}1s \rightarrow \sigma^*(\text{CC})$ resonant transitions, respectively, where the C_F and C_N denote the carbon atoms forming the CF_3 and CN groups in CF_3CN . These assignments are also supported by the angle-resolved mass spectroscopy discussed in the next section. The peak assignments are indicated by bars in the top panel of Fig. 1 where the ionization potentials for the $\text{C}_\text{N}1s$ and $\text{C}_\text{F}1s$ core electrons have not been reported and then they were estimated to be 294.1 and 299.8 eV [38, 39].

Total ion yield spectrum of CF_3CN in the N K-shell region is shown in the bottom panel of Fig. 1 with the peak assignments [40]. That is, the strongest peak at 400 eV is assignable to the $\text{N}1s \rightarrow \pi^*(\text{CN})$ resonant transition. Some peaks around 409 eV are exposed by the least-squares curve fitting with Gaussian functions and their assignments are shown in the figure. The peak assignments are basically consistent with those for the $\text{N}1s$ transition of CH_3CN [41]. In the following sections we discuss the reaction dynamics of CF_3CN by exciting the C_F , C_N and N K-shell electrons at some selected resonant states that are assigned in Fig. 1.

3.1.2. Angle-resolved mass spectra and reaction dynamics

(1) N K-shell excitation

The studies on reaction dynamics of diatomic molecules [4-10] have shown that an angle-resolved photofragmentation is characteristically observed by exciting a core electron into the vacant π^* level. Figure 2 shows the L-TOF mass spectra observed in the $\text{N}1s \rightarrow \pi^*(\text{CN})$ transition at 400 eV [40]. The mass spectrum in the top panel was measured by locating the ion detector in the direction perpendicular to the linearly polarized electric vector of synchrotron radiation while that in the bottom panel was detected in the parallel direction. It is remarkable that the peak shapes of the CN^+ , CF_2^+ and CF_3^+ ions observed in the perpendicular direction show two ‘wings’. The wing in the low-mass region originates from the ions with kinetic energies initially moving toward the ion detector. The wing in the high-mass region originates in the ions with kinetic energies initially moving away from the ion detector and repelled back toward the ion detector by the applied electric field. The central peak is produced by the ions with zero or small kinetic energies. The fragment ions with kinetic energies initially moving in a direction parallel to the electric vector of synchrotron radiation cannot reach the ion detector located at the perpendicular position.

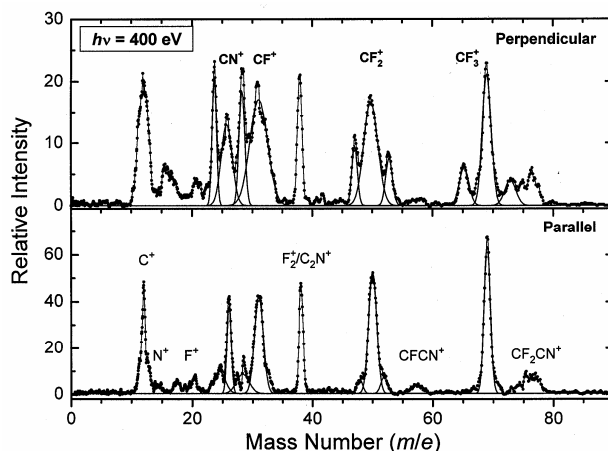


Figure 2. Angle-resolved L-TOF mass spectra of CF_3CN observed in the $\text{N}1s \rightarrow \pi^*(\text{CN})$ transition at 400 eV. Perpendicular (top panel) and parallel directions (bottom panel). The dots are the experimental data. The solid curves are only to facilitate the readability of two ‘wings’ for the CN^+ , CF^+ , CF_2^+ and CF_3^+ fragment ions.

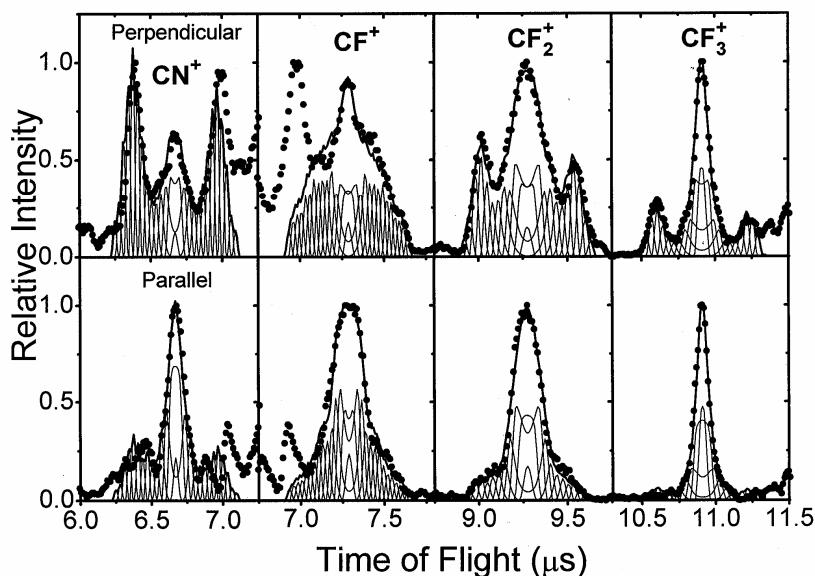


Figure 3. Experimental and calculated angle-resolved L-TOF mass spectra of CF_3CN in the $\text{N1s} \rightarrow \pi^*(\text{CN})$ transition at 400 eV. Perpendicular (top panels) and parallel directions (bottom panels). The dots are the experimental data. The thin solid curves are the calculated profiles for the kinetic energies of 0.01–5.34 eV (CN^+), 0.01–3.17 eV (CF^+), 0.01–2.02 eV (CF_2^+) and 0.01–2.02 eV (CF_3^+). The thick curve is the sum of the thin curves.

The profiles of the fragment ions were reproduced by using a fitting method [42], in which the kinetic energies of a fragment ion and the β parameters in Eq. (1) were determined so as to minimize the difference between the observed data and the calculated peak profile. In these calculations the photons were assumed to be 100% linearly polarized since the degree of linear polarization was measured to be better than 98% [43]. Figure 3 shows the typical L-TOF mass spectra at the $\text{N1s} \rightarrow \pi^*(\text{CN})$ excitation obtained by this fitting method: The anisotropy parameters deduced for the CN^+ , CF_3^+ and CF_2^+ ions are tabulated in Table 1 with those found in the C K-shell excitation at 286.7 and 296.5 eV. It is clear that the largest negative values of the energetic CN^+ , CF_3^+ and CF_2^+ fragment ions formed at 400 eV are $\beta = -1.0$, -0.96 and -0.98 , respectively, being close to the expected $\beta = -1$ in Eq. (1) for the pure $\Sigma - \Pi$ transition. The β values of the CF^+ ion at 400 eV were $\beta = +0.37$, -0.56 and -0.80 in the kinetic energy (KE) regions $\text{KE} = 0.01 - 0.21$ eV, $0.34 - 0.88$ eV and $1.12 - 3.17$ eV, respectively [40]. The kinetic energy distributions of the fragment ions are shown in Fig. 4 where the curves are obtained by the least-squares curve fitting with Gaussian functions. We see that most of the CN^+ , CF_3^+ and CF_2^+ ions with kinetic energies are ejected in the direction perpendicular to the linear electric vector of synchrotron radiation since $\beta \cong -1.0$. The CF_3CN molecules excited to the resonant $\pi^*(\text{CN})$ state are highly expected to be populated in the final states of +1 charged ions in various degrees of decay channels, and then they decompose into $\text{CF}_3^+ + \text{CN}$, $\text{CF}_3 + \text{CN}^+$, $\text{CF}_2^+ + \text{CN}$ or $\text{CF}_2 + \text{CN}^+$. The maximum kinetic energy distribution of the CN^+ ion is about 3 eV (see

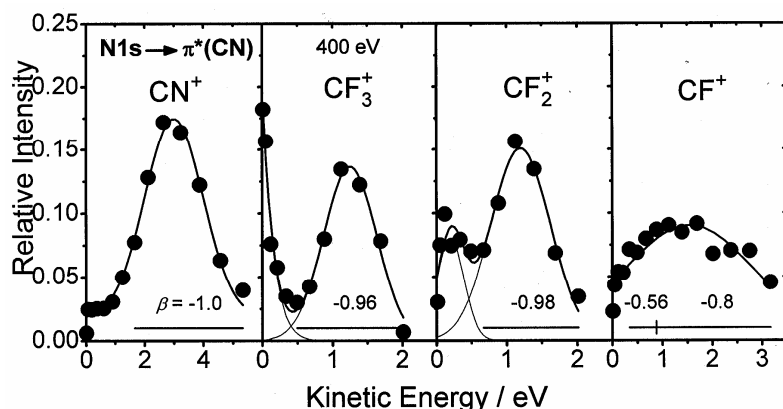


Figure 4. Kinetic energy distributions of the CN^+ , CF^+ , CF_2^+ and CF_3^+ fragment ions formed by exciting CF_3CN in the $\text{N}1s \rightarrow \pi^*(\text{CN})$ transition at 400 eV. The solid curves were obtained by the least-squares curve fitting with Gaussian functions. The β values for the energetic fragment ions are indicated.

Fig. 4). On the assumption of the axial recoil approximation in the dissociation of the $\text{F}_3\text{C}-\text{CN}$ chemical bond, the kinetic energy of CF_n^+ ($n = 2, 3$) is estimated by the following simple expression:

$$\text{KE}_{\text{est}}(\text{CF}_n^+) = 3 \text{ (eV)} \times M(\text{CN})/M(\text{CF}_n) \quad (2)$$

where the $M(\text{CN})/M(\text{CF}_n)$ is the mass ratio between the CN^+ and CF_n^+ fragment ions. The estimated KE_{est} for CF_3^+ and CF_2^+ are 1.1 and 1.6 eV, respectively, which are basically in agreement with the experimental peak maxima of $\text{KE} = 1.2$ eV in Fig. 4. When the ionization and vibrational excitation simultaneously occur at the CF_3 group, the CF^+ fragment ion can be produced through two C–F bonds cleavage. In this case the formed CF^+ ion would be ejected into several directions with different kinetic energies. Actually, the kinetic energy distribution of CF^+ is relatively wide and flat with smaller negative β values as shown in the right panel of Fig. 4.

(2) C K-shell excitation

The angle-resolved L-TOF mass spectra of CF_3CN were measured in the C K-shell region [38] and the fitting analysis [42] was performed similarly to the $\text{N}1s$ excitation. The kinetic energy distributions of the CN^+ , CF_3^+ and CF_2^+ fragment ions are shown in Fig. 5 for the excitation of the $\text{C}_{\text{N}}1s$ electron into the $\pi^*(\text{CN})$ level at 286.7 eV and those of the $\text{C}_{\text{F}}1s$ electron excited into $\pi^*(\text{CN})$ and $\sigma^*(\text{CF})$ at 295.1 and 296.5 eV, respectively [38]. In these kinetic energy distributions at the C K-edge, the simple expression (2) is again valid in forming the energetic fragment ions.

For the $\text{C}_{\text{N}}1s \rightarrow \pi^*(\text{CN})$ excitation in the top panels of Fig. 5, the approximated $\Delta\lambda = \pm 1$ transition character is reflected more in the angular distribution of the energetic CN^+ ($\beta = -0.46$) than CF_3^+ (-0.2). In the middle panels of Fig. 5 for the neighboring $\text{C}_{\text{F}}1s$ excitation to the $\pi^*(\text{CN})$ level, the approximate $\Delta\lambda = \pm 1$ character appears stronger in

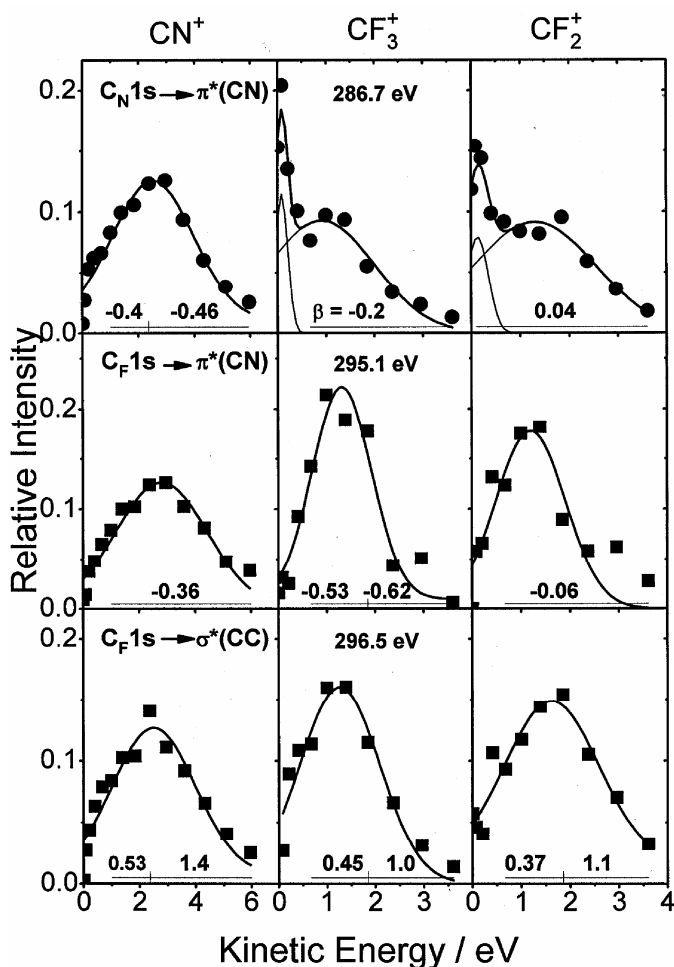


Figure 5. Kinetic energy distributions of the CN^+ , CF_3^+ and CF_2^+ fragment ions observed by site-selective excitation of the $\text{C}_\text{N}1\text{s}$ and $\text{C}_\text{F}1\text{s}$ electrons of CF_3CN . The solid circles are the data for the $\text{C}_\text{N}1\text{s} \rightarrow \pi^*(\text{CN})$ transition at 286.7 eV, and the solid squares are those for the $\text{C}_\text{F}1\text{s}$ excitation of the CF_3 group to $\pi^*(\text{CN})$ and $\sigma^*(\text{CC})$ at 295.1 and 296.5 eV, respectively.

the CF_3^+ ejection than the CN^+ channel since the anisotropy parameter of the energetic CF_3^+ ion was $\beta = -0.62$ and that of CN^+ was -0.36 [38]. However, the β values of these two $\text{C}_\text{N}1\text{s}$ and $\text{C}_\text{F}1\text{s}$ electrons excitation into the $\pi^*(\text{CN})$ state are smaller than the expected $\beta = -1$. This finding suggests that the bending motion of the $\text{C}-\text{C}\equiv\text{N}$ molecular skeleton is probably excited at the same time with the $\text{C}-\text{C}$ bond cleavage. The anisotropy parameters of the energetic CN^+ , CF_3^+ and CF_2^+ formed at 296.5 eV were $\beta = +1.4$, $+1.0$ and $+1.1$, respectively, being consistent with the assignment to the $\text{C}_\text{F}1\text{s} \rightarrow \sigma^*(\text{CC})$ transition (see Table 1 and the bottom panels of Fig. 5).

Table 1. The β values obtained by a fitting method^a for CN^+ , CF_3^+ and CF_2^+ at 400, 286.7 and 296.5 eV.

Photon energy (eV)	CN^+		CF_3^+		CF_2^+	
	β	KE ^b	β	KE	β	KE
400.0	-0.43	0.01 – 0.37	-0.27	0.01 – 0.34	-0.19	0.01 – 0.21
$\text{N1s} \rightarrow \pi^*(\text{CN})$	-0.71	0.61 – 1.25	-0.96	0.49 – 2.02	-0.8	0.34 – 0.67
	-1.0	1.66 – 5.34			-0.98	0.88 – 2.02
286.7	-0.07	0.01 – 0.67	-0.03	0.01 – 0.41	0.03	0.01 – 0.41
$\text{C}_\text{N}1\text{s} \rightarrow \pi^*(\text{CN})$	-0.4	1.0 – 2.37	-0.2	0.67 – 1.85	0.04	0.67 – 4.37
	-0.46	2.69 – 6.86	-0.21	2.37 – 4.37		
296.5	0.29	0.01 – 0.67	0.42	0.01 – 0.41	0.32	0.01 – 0.41
$\text{C}_\text{F}1\text{s} \rightarrow \sigma^*(\text{CC})$	0.53	1.0 – 2.37	0.45	0.67 – 1.85	0.37	0.67 – 1.85
	1.4	2.69 – 6.86	1.0	2.37 – 4.37	1.1	2.37 – 4.37

^a See Ref. 42.^b Kinetic energy in eV.

3.1.3. Site-dependent photofragmentation competing with intramolecular energy relaxation

The kinetic energy distributions of the CF_3^+ and CF_2^+ fragment ions formed at the N1s electron excitation give the peaks with low energy components as shown in Fig. 4. The relative contributions of the low kinetic energy components of the CF_n^+ ($n = 2, 3$) ions are about 20% at the terminal N1s excitation. The yields with low kinetic energies decrease from $\approx 10\%$ to 0% by changing the excitation site from the central $\text{C}_\text{N}1\text{s}$ to another terminal $\text{C}_\text{F}1\text{s}$ electron (see Fig. 5). This observation means that the kinetic energy distributions of the fragment ions depend on the site of excitation. There should be at least two pathways for the formation of CF_n^+ ($n = 2, 3$). By contrast the profile of the kinetic energy distribution of CN^+ is approximated with a single function at any excitation site. These findings are reasonably understood by considering fragmentation competing with intramolecular energy relaxation. That is, the fragmentation into CF_n^+ following the N1s excitation competes with the intramolecular energy flow from the initially excited K-shell electron to the CF_3 group with molecular vibrational modes. We think that large parts of the CF_n^+ ions (about 80%) are formed directly with the higher kinetic energies and ejected into the direction perpendicular to the linear electric vector of synchrotron radiation. Some CF_n^+ ions ($\approx 20\%$) with lower kinetic energies are produced after energy redistribution via the $\text{C-C}\equiv\text{N}$ skeleton into the vibrational modes of CF_3 and then ejected into an isotropic direction with the β values close to zero.

When the C K-shell electron of the CF_3 group is initially excited, energy flow from the CF_3 group to the terminal N atom would occur. However, the CN group is not an effective energy reservoir since it has only one vibrational mode. Actually the CN^+ ion gives one peak in the kinetic energy distribution. Excitation of the central C K-shell electron of the CN group lies in the middle situation between the terminal N1s and $\text{C}_\text{F}1\text{s}$ excitations.

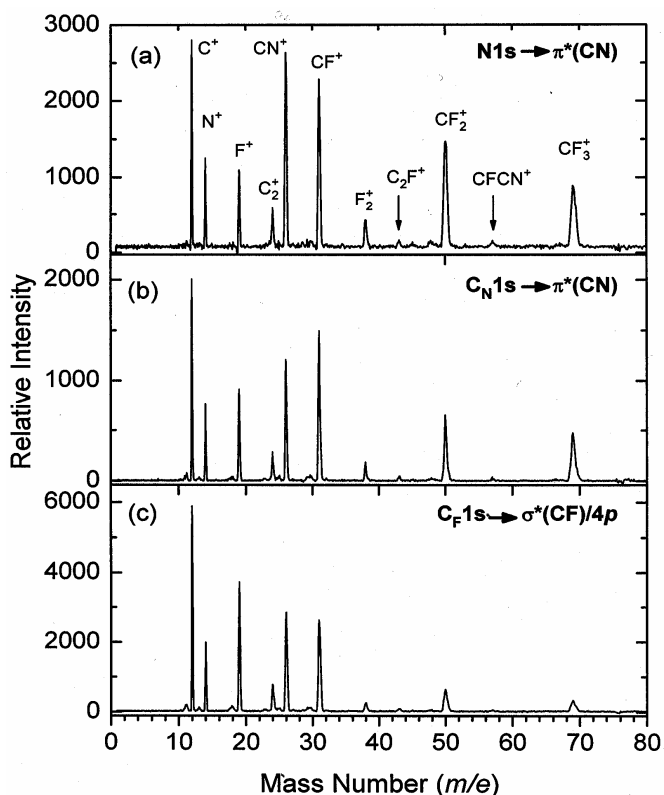


Figure 6. Reflectron type TOF mass spectra of CF_3CN observed by exciting the terminal $\text{N}1\text{s}$, central $\text{C}_\text{N}1\text{s}$ and another terminal $\text{C}_\text{F}1\text{s}$ electron.

Figure 6 shows the reflectron type time-of-flight (R-TOF) mass spectra measured at the different sites: $\text{N}1\text{s} \rightarrow \pi^*(\text{CN})$ at 400 eV, $\text{C}_\text{N}1\text{s} \rightarrow \pi^*(\text{CN})$ at 286.7 eV and $\text{C}_\text{F}1\text{s} \rightarrow \sigma^*(\text{CF})/4p$ at 298.7 eV [38]. In these experiments, the R-TOF mass spectrometer was fixed at the magic angle. The relative yields of the fragment ions are summarized in Table 2 after subtraction of the contribution of the valence electron excitation [38]. The main products CN^+ and CF^+ with the yields of $\approx 20\%$ are little dependent on the excitation site. The yields of the large CF_n^+ ($n = 2, 3$) fragment ions decrease to about one third by changing the excitation site from the $\text{N}1\text{s}$ to $\text{C}_\text{F}1\text{s}$ electron. The distribution of the large fragment ions at the central $\text{C}_\text{N}1\text{s}$ excitation lies again in the middle of the $\text{N}1\text{s}$ and $\text{C}_\text{F}1\text{s}$ extremes. The formation of F_2^+ is noticeable since this fragment ion is formed through simultaneous two C-F bonds dissociation following energizing the CF_3 bending mode. The amount of F_2^+ is small but it decrease down to 60% by moving the excitation site from the N K-shell to C_F K-shell electron. That is, the CF_3 group acts as a reservoir of intramolecular energy supplied from the initially excited $\text{N}1\text{s}$ and then forms the F_2^+ ion, being consistent with the discussion of the kinetic energy distribution just above.

Table 2. Yields of fragment ions (%) for site-specific excitation of CF₃CN.

Fragment ion	N1s → π*(CN) 400 eV	C _N 1s → π*(CN) 286.7 eV	C _F 1s → σ*(CF)/4p 298.7 eV
N ⁺	4.3	5.7	7.0
F ⁺	4.8	9.7	18.0
C ⁺	9.0	13.0	18.4
C ₂ ⁺	3.1	3.4	5.0
CN ⁺	19.5	15.5	18.1
CF ⁺	18.8	21.4	20.0
F ₂ ⁺	3.4	2.4	2.0
CF ₂ ⁺	21.0	13.2	7.0
CF ₃ ⁺	16.1	15.7	4.5

3.2. CF₃CCH excited at the C K-shell electron

Total photoabsorption cross section of CF₃CCH is shown in Fig. 7. The details of the peak assignments were given elsewhere [44]. The spectral features are basically similar to those of CF₃CN in the top panel of Fig. 1. The ionization potentials for the C1s electrons of the CF₃ (denoted by C_F1s), the central C (C_C1s) and the CH group (C_H1s)

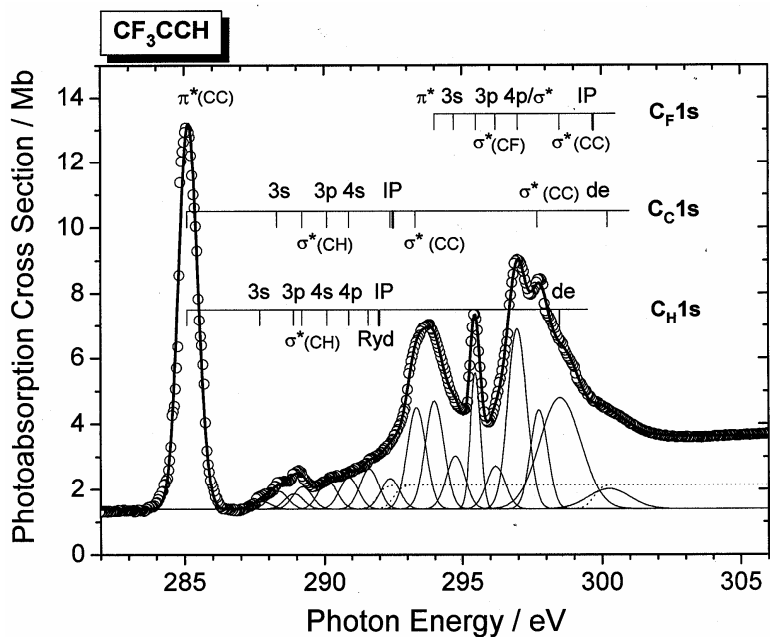


Figure 7. Total photoabsorption cross section of CF₃CCH in the C K-shell region. The open circles are the experimental data and the solid curves were obtained by the least-squares curve fitting. The “de” means double excitation.

were estimated to be 299.7, 292.5 and 292.0 eV [44] from the published IP values of hydrocarbons [45]. By using these estimated IP's, the peak assignments are shown in Fig. 7. Resonant transitions of the C_H1s and C_C1s electrons are heavily overlapped. Thus, we excited the $C1s$ electrons of the CCH group (denoted by $C_{CCH}1s$) and CF_3 group by tuning the soft X-ray energies to 285.1 and 295.4 eV, respectively. The L-TOF mass spectra were observed by locating the ion detector in the direction perpendicular or parallel to the linear electric vector of synchrotron radiation. The energetic C_2H^+ and CF_3^+ ions were ejected into the parallel direction in the $C_F1s \rightarrow \sigma^*(CF)$ transition at 295.4 eV while those formed in the $C_{CCH}1s \rightarrow \pi^*(CC)$ excitation at 285.1 eV were ejected into the perpendicular direction [44].

Maxima of the kinetic energies of CH^+ and C_2H^+ produced at the $C_F1s \rightarrow \sigma^*(CF)$ transition were found to be 3.6 and 2.5 eV, respectively, as shown in the upper panels of Fig. 8. The kinetic energy distribution of CF_3^+ has two peaks at $KE \cong 0.6$ and 1.3 eV, which correspond to the $CF_3^+ + CH^+$ (or CH) and $CF_3^+ + C_2H^+$ (or C_2H) dissociation channels since the mass ratios of $M(CH)/M(CF_3) \cong 0.2$ and $M(C_2H)/M(CF_3) \cong 0.4$ are close to the ratios of KE maxima: $0.6/3.6 \cong 0.2$ and $1.3/2.5 \cong 0.5$, respectively. The kinetic

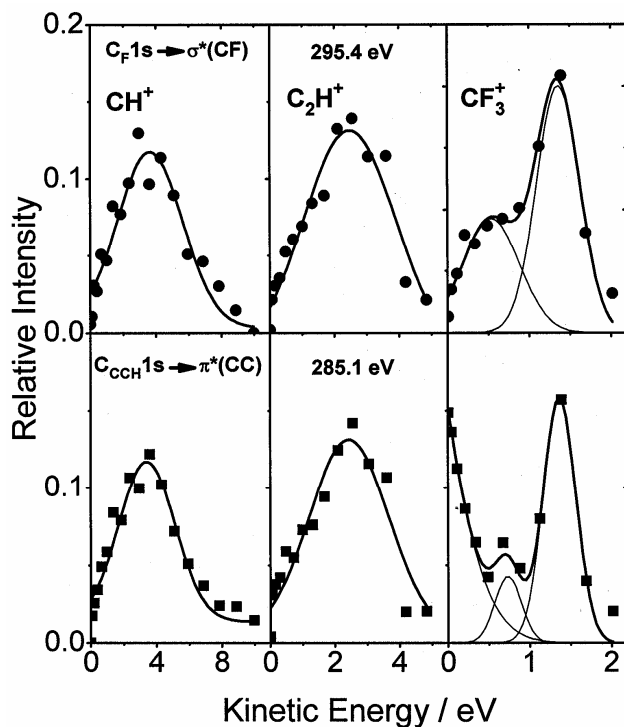


Figure 8. Kinetic energy distributions of the CH^+ , C_2H^+ and CF_3^+ fragment ions observed by exciting the $C1s$ electron of CF_3CCH . The solid circles indicate the results at the $C_F1s \rightarrow \sigma^*(CF)$ transition and the solid squares are those at the $C_{CCH}1s \rightarrow \pi^*(CC)$ excitation. The thin curves in CF_3^+ were obtained by the least-squares curve fitting with Gaussian functions. The thick curve is the sum of the thin ones.

energy distribution profile of CF_3^+ in the $\text{C}_{\text{CCH}}1s \rightarrow \pi^*(\text{CC})$ transition at 285.1 eV is largely different from that in the $\text{C}_{\text{F}}1s \rightarrow \sigma^*(\text{CF})$ excitation: The peaks with the maxima at $\text{KE} \approx 0.7$ and 1.3 eV should correspond to the $\text{CF}_3^+ + \text{CH}^+$ (or CH) and $\text{CF}_3^+ + \text{C}_2\text{H}^+$ (or C_2H) breakdown pathways discussed above. The component peaked at $\text{KE} = 0$ eV can be understood by the intramolecular energy relaxation just as discussed in the previous CF_3CN section. That is, when the $\text{C}_{\text{F}}1s$ electron is excited, the CF_3^+ fragment ions are spontaneously produced with $\text{KE} \approx 0.6$ and 1.3 eV depending on the counterpart CH^+ (or CH) and C_2H^+ (or C_2H), respectively. At the $\text{C}_{\text{CCH}}1s$ excitation the CF_3^+ fragment ion is formed and at the same time a part of excess energy is distributed into the vibrational modes of CF_3 . That is, the CF_3 group in CF_3CCH works as an effective energy reservoir. The CF_3^+ fragment ions generated after the energy redistribution should have small kinetic energy. Of course excess energy would flow from the initially excited $\text{C}_{\text{F}}1s$ to the terminal CH group. However, the CH group has only one vibrational mode and then it is not an effective energy reservoir. The CH^+ and C_2H^+ fragment ions do not have a low $\text{KE} \approx 0$ component as shown in Fig. 8.

4. Molecular size effects on the site-specific photo-fragmentation of N and O K-shell excited $\text{CH}_3\text{CO}(\text{CH}_2)_n\text{CN}$ ($n = 0-3$)

In the previous sections we discussed the fragmentation of the K-shell excited CF_3CN and CF_3CCH which competes with intramolecular energy flow from the initially excited atom to the terminal group with vibrational modes. We have shown that the kinetic energy distributions of the fragment ions depend on the site of excitation in the molecules. We anticipated thus that the effective area of site-specific fragmentation caused by the Coulomb explosion of a K-shell excited molecule would be estimated by changing the length of molecule. In this section the molecular size effect was investigated by successively inserting a CH_2 group between the CO and CN functional groups in a series of $\text{CH}_3\text{CO}(\text{CH}_2)_n\text{CN}$ and then selectively exciting the O and N K-shells.

4.1. Photoabsorption spectra

Total photoabsorption cross sections of $\text{CH}_3\text{CO}(\text{CH}_2)_n\text{CN}$ ($n = 0-3$) are shown in Figs. 9 and 10 in the N and O K-shell regions, respectively [30]. The spectra of CH_3COCN have some structures both in the N and O K-edges, the details of which were assigned in the recent paper [30]. Two π^* orbitals are spread over the CH_3COCN molecule and then the two peaks at 398.1 and 399.5 eV were assigned to the excitation of the N1s electron into the $\pi^*(\text{CO})$ and $\pi^*(\text{CN})$ vacant orbitals, respectively. Some Rydberg transitions were observed in the regions of 402-405 eV and 535-539 eV [30]. The deconvoluted peaks for CH_3COCN by use of the least-squares fitting are shown by thin curves in the top panels of Figs. 9 and 10.

The strong peaks around 400 eV in Fig. 9 and 530.5 eV in Fig. 10 are assigned to the $\text{N}1s \rightarrow \pi^*(\text{CN})$ and $\text{O}1s \rightarrow \pi^*(\text{CO})$ transitions, respectively, for the $n = 0-3$ compounds. The weak and broad bands around 420 eV in Fig. 9 are assignable to the $\text{N}1s \rightarrow \sigma^*(\text{CN})$ transitions, and those around 545 eV in Fig. 10 are the $\text{O}1s \rightarrow \sigma^*(\text{CO})$ excitations.

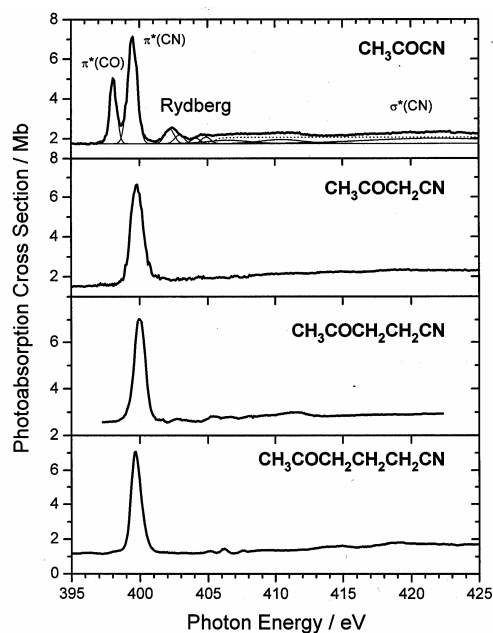


Figure 9. Total photoabsorption cross sections of $\text{CH}_3\text{CO}(\text{CH}_2)_n\text{CN}$ ($n = 0-3$) in the N1s regions. The thin curves in CH_3COCN were obtained by the least-squares curve fitting. The details are given in Ref. 30.

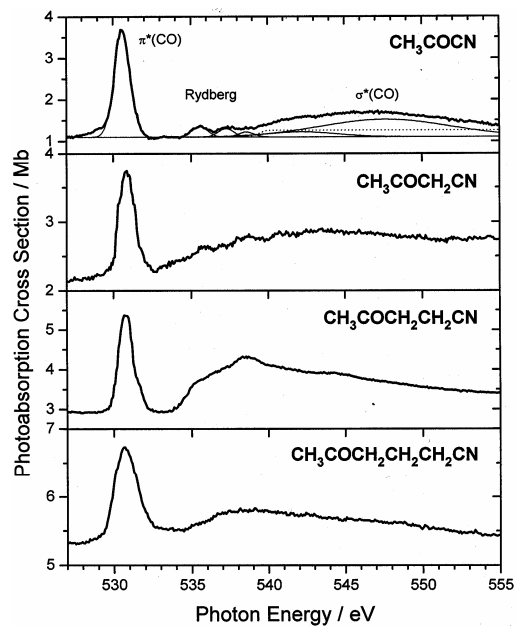


Figure 10. Total photoabsorption cross sections of $\text{CH}_3\text{CO}(\text{CH}_2)_n\text{CN}$ ($n = 0-3$) in the O1s regions. The thin curves in CH_3COCN were obtained by the least-squares curve fitting. The details are given in Ref. 30.

4.2. Site-specific photofragmentation

Reflectron type TOF mass spectra were measured by tuning soft X-rays to the $\pi^*(\text{CN})$ at ≈ 400 eV, $\pi^*(\text{CO})$ around 530 eV and the direct ionization of $\text{N}1s^{-1}$ and $\text{O}1s^{-1}$ for the $\text{CH}_3\text{CO}(\text{CH}_2)_n\text{CN}$ ($n = 0-3$) compounds. Figure 11 shows the R-TOF mass spectra of $\text{CH}_3\text{CO}(\text{CH}_2)_2\text{CN}$ after correcting the contribution of valence electrons [30]. The yields of $m/e = 14$ ($\text{CH}_2^+ + \text{N}^+$) and 26 ($\text{C}_2\text{H}_2^+ + \text{CN}^+$) at the N K-shell excitation are, respectively, 2.0 and 1.7 times as much as those at the O K-edge, being due to the selective ionization of the $(\text{CH}_2)_2\text{CN}$ group by the N1s electron excitation. One of the prominent products at the O K-shell excitation is CH_3CO^+ , being 1.9 times as much as the yield at the N K-edge. However, we do not think that these differences between the N and O K-shell excitations are clear site-dependent photofragmentation. These differences in site-specific photofragmentation of $\text{CH}_3\text{CO}(\text{CH}_2)_n\text{CN}$ by exciting the N and O K-shells were little for $n \leq 2$. In addition, fragmentation patterns depending on the excited states such as the π^* , direct ionization, Rydberg and σ^* states were nearly the same in the excitation of the N and O K-edges for $n = 0-2$.

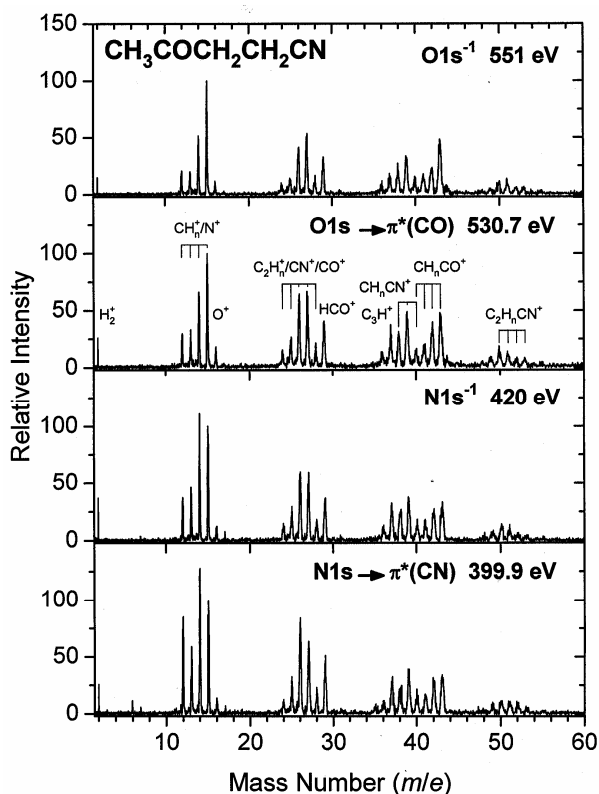


Figure 11. Reflectron type TOF mass spectra of $\text{CH}_3\text{CO}(\text{CH}_2)_2\text{CN}$ observed by exciting the O and N K-shells. The number of hydrogen atoms are $n = 0-2$ for CH_nCN^+ ; $n = 0-3$ for CH_n^+ , CH_nCO^+ and $\text{C}_2\text{H}_n\text{CN}^+$; and $n = 0-4$ for C_2H_n^+ .

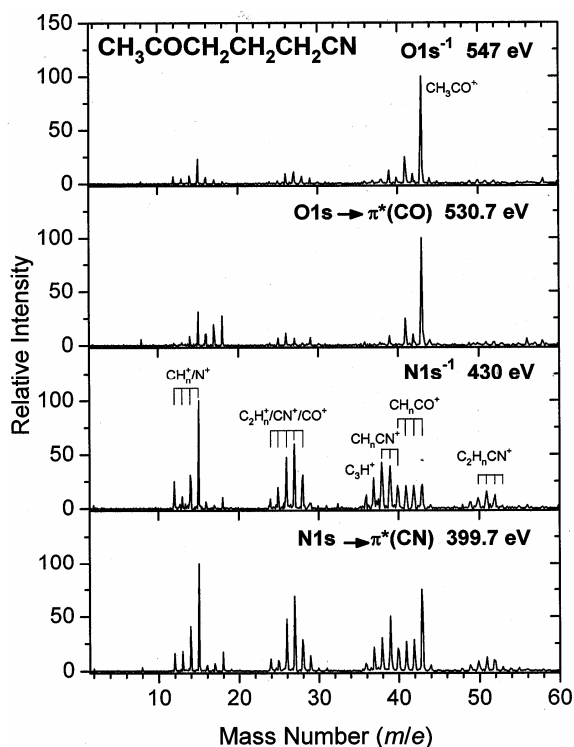


Figure 12. Reflectron type TOF mass spectra of $\text{CH}_3\text{CO}(\text{CH}_2)_3\text{CN}$ observed by exciting the O and N K-shells. The number of hydrogen atoms are $n = 0-2$ for CH_nCN^+ ; $n = 0-3$ for CH_n^+ , CH_nCO^+ and $\text{C}_2\text{H}_n\text{CN}^+$; and $n = 0-4$ for C_2H_n^+ .

Reflectron type TOF mass spectra of the longest $\text{CH}_3\text{CO}(\text{CH}_2)_3\text{CN}$ molecule are shown in Fig. 12 [30]. Formation of CH_3CO^+ at the O1s electron excitation clearly overwhelms others and the yield reaches to 37% of the total ions produced. By contrast many kinds of small fragment ions are produced via the N K-shell excitation. The CH_3^+ fragment ion gives the highest yield, being 10% of the total products. The fragment ions with mass numbers $m/e = 15$ (CH_3^+), 16 (O^+) and 41–43 (CH_nCO^+) clearly originate in the CH_3CO group of the parent molecule. Thus, we define the sum of them as “O-side products”. The fragment ions at the $m/e = 24-27$ (CN^+ and C_2H_n^+ , $n = 0-3$), 38–39 (CH_nCN^+ , $n = 0, 1$) and 50–53 ($\text{C}_2\text{H}_n\text{CN}^+$, $n = 0-3$) undoubtedly originate in the $(\text{CH}_2)_3\text{CN}$ group of $\text{CH}_3\text{CO}(\text{CH}_2)_3\text{CN}$, and thus we denote the sum of them by “N-side products”. Table 3 gives the yields of “O-side products” and “N-side products” for $\text{CH}_3\text{CO}(\text{CH}_2)_n\text{CN}$ ($n = 2, 3$) [30]. The yield of “O-side products” at the O1s excitation for $n = 3$, $\text{CH}_3\text{CO}(\text{CH}_2)_3\text{CN}$, reaches 62% of the total fragment ions and decreases to 28% at the N1s excitation. The yield of “N-side products” increases from 17% to 40% by changing the excitation site from O1s to N1s. These observations for $n = 3$ are in contrast to the results for $n = 2$, $\text{CH}_3\text{CO}(\text{CH}_2)_2\text{CN}$, which do not show characteristic distributions in Table 3. That is, shortening one CH_2 segment increases miscellaneous fragment ions which are difficult to be assigned to the N-side or O-side products.

Table 3. Fragment ions grouped into the O- and N-atoms sides at the O and N K-shell excited $\text{CH}_3\text{CO}(\text{CH}_2)_n\text{CN}$ ($n = 2, 3$). The yields are given in %.

	n = 2		n = 3	
	O1s ^c	N1s ^d	O1s	N1s
O-side products ^a	30	23	62	28
N-side products ^b	39	32	17	40

^a The sum of fragment ions at $m/e = 15, 16$ and $41-43$.

^b The sum of fragment ions at $m/e = 24-27, 38-39$, and $50-53$.

^c O K-shell excitation.

^d N K-shell excitation.

Auger electron emission follows the K-shell excitation. In this process a positive hole in the K-shell is occupied by a valence electron and then the hole moves to a valence molecular orbital to break a chemical bond. Thus, the characters of valence molecular orbitals may give the difference in the product distributions shown in Table 3. The configurations of some valence molecular orbitals representation in the ground states of $n = 2$ and 3 for $\text{CH}_3\text{CO}(\text{CH}_2)_n\text{CN}$ are expressed by the following [30]:

$$\begin{aligned}
 n = 2: & \quad \dots(3a'')^2(4a'')^2(12a')^2(13a')^2(5a'')^2(14a')^2 \\
 n = 3: & \quad \dots(4a'')^2(5a'')^2(14a')^2(15a')^2(6a'')^2(16a')^2
 \end{aligned}$$

where the core orbitals are ignored in the numbering scheme. The outermost $14a'$ and $16a'$ molecular orbitals are the σ -HOMOs localized on the CH_3CO group. The molecular orbitals of $5a''-12a'$ for $n = 2$ and $6a''-14a'$ for $n = 3$ are strongly localized on the $(\text{CH}_2)_n\text{CN}$ group. The valence orbitals inner than $4a''$ or $5a''$ are spread over the molecule. The characters of the valence molecular orbitals whose electrons participate in Auger decays are similar between the two compounds. Thus, the mass spectra of $\text{CH}_3\text{CO}(\text{CH}_2)_n\text{CN}$ after the Auger electron emission are expected to be similar between $n = 2$ and 3 . From this consideration we believe that the characters of the valence molecular orbitals have little relation with the site-specific fragmentation in Table 3.

The site-dependent decomposition observed probably results from the intramolecular energy relaxation which competes with bond dissociation: Throughout $\text{CH}_3\text{CO}(\text{CH}_2)_n\text{CN}$ ($n = 0-3$), the yield of CH_3CO^+ at the O K-shell excitation was superior to that at the N K-edge [30]. The O1s electron is initially excited and then the OC-C bond is preferentially broken after Auger electron emission. A part of the intramolecular excess energy would be distributed into vibrational modes of the $(\text{CH}_2)_n\text{CN}$ ($n = 0-3$) group in the Auger decays, just as discussed in the CF_3CN and CF_3CCH sections. The high yield of CH_3CO^+ in $n = 3$ can be reasonably understood if the vibrational modes of $(\text{CH}_2)_3\text{CN}$ act as an effective energy reservoir for the energy flow from the initially excited O1s toward the CN terminal. The number of freedom in the vibrational modes of $(\text{CH}_2)_3\text{CN}$ would be critical to suppress fragmentation of $(\text{CH}_2)_3\text{CN}$ into small ions. This explanation is useful to understand the fragmentation pattern at the N1s excitation: The $(\text{CH}_2)_3\text{CN}$ group acts as a barrier of energy flow from

the initially excited N1s to CH_3CO and simultaneously decomposes into small fragment ions to produce the “N-side products” composed of C_2H_n^+ , CN^+ , CH_nCN^+ , $\text{C}_2\text{H}_n\text{CN}^+$, and so forth. For the molecules of $\text{CH}_3\text{CO}(\text{CH}_2)_n\text{CN}$ ($n \leq 2$), the number of vibrational modes would be insufficient to keep the $(\text{CH}_2)_n\text{CN}$ group being an efficient energy reservoir. The $(\text{CH}_2)_n\text{CN}$ ($n \leq 2$) group decomposes into ionic fragments at both the N and O K-shell excitation and then the site-specific fragmentation becomes vague.

5. Angle-resolved photofragmentation of C K-shell excited CF_2CH_2

We discuss the reaction dynamics of the K-shell excited small molecule, CF_2CH_2 . Figure 13 shows the total photoabsorption cross section of CF_2CH_2 in the C1s region. The distinct peaks at 285.3 and 289.6 eV have been assigned to the excitation of the C1s electrons of the CH_2 and CF_2 groups into the $\pi^*(\text{CC})$ vacant orbital, respectively, by McLaren et al who used electron energy loss spectroscopy [46]. The 3s and 3p Rydberg transitions have been also assigned in their paper. The total photoabsorption cross sections at the two $\pi^*(\text{CC})$ peaks are 3.0 and 7.6 Mb after subtraction of the contribution of valence electrons. These two values are in agreement with the published data of 3.3 and 8.0 Mb [46].

The shapes of the two $\pi^*(\text{CC})$ peaks are obviously asymmetric. The vibrational spacing $\nu = 0.4$ eV is embedded in the peaks when we analyze the spectrum by use of the least-squares curve fitting with Gaussian functions. The vibrational mode is probably the CH stretching or overtone of the CCH or CCF bending. We measured the angle-resolved L-TOF mass spectra at 285.3 and 289.6 eV and then deduced the kinetic energies and β values of the CH_2^+ , F^+ and CF_2^+ fragment ions by using the method described in the CF_3CN section. The results are shown in Fig. 14 where the kinetic

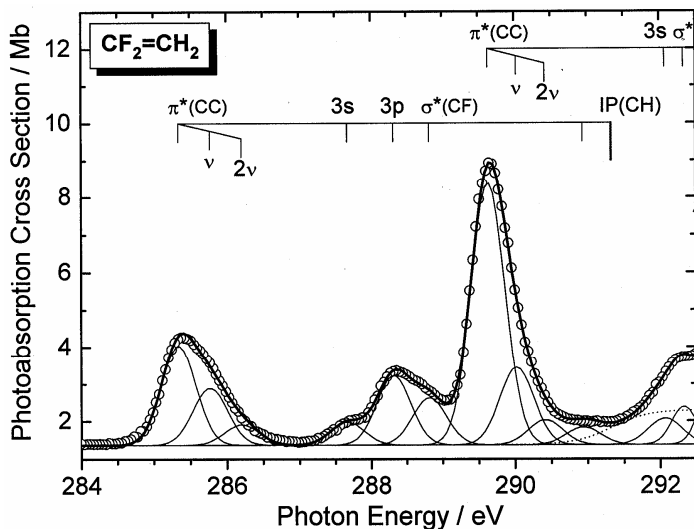


Figure 13. Total photoabsorption cross sections of CH_2CF_2 in the C1s region. The solid curves were obtained by the least-squares curve fitting.

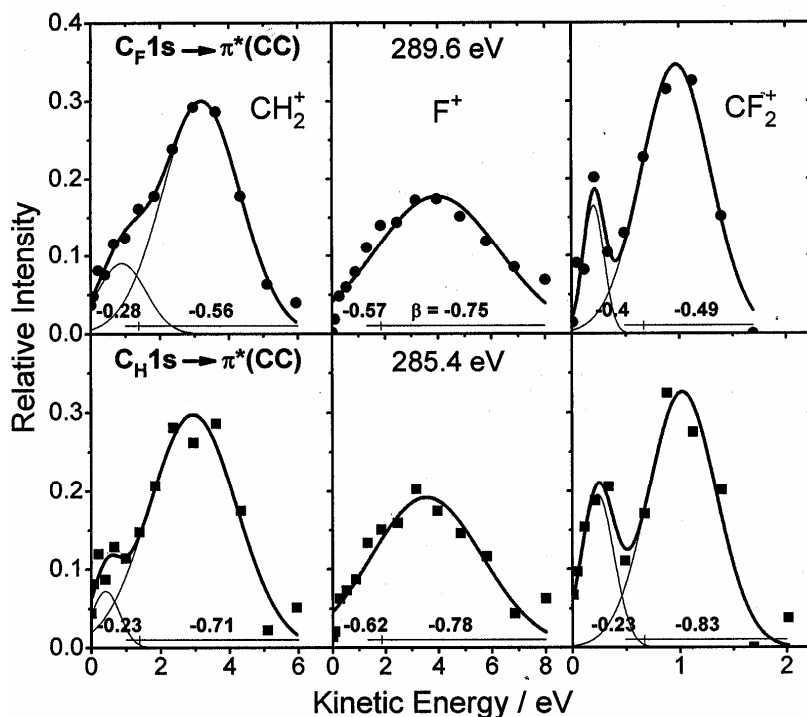


Figure 14. Kinetic energy distributions of the CH_2^+ , F^+ and CF_2^+ fragment ions observed by exciting the $\text{C}1s$ electron of CH_2CF_2 . The solid circles indicate the results at the $\text{C}_F1s \rightarrow \pi^*(\text{CC})$ transition and the solid squares are those at the $\text{C}_H1s \rightarrow \pi^*(\text{CC})$ excitation. The thin curves in CH_2^+ and CF_2^+ were obtained by the least-squares curve fitting with Gaussian functions. The thick curve is the sum of the thin ones.

energy distributions of CF_2^+ and CH_2^+ are best fitted by two Gaussian functions while that of F^+ is done by a single function. The maxima of the main peaks for the CH_2^+ and CF_2^+ ions produced at 289.6 eV are found to be 3.2 and 0.97 eV, respectively. The ratio of these kinetic energies ($0.97/3.2 = 0.3$) is close to the mass ratio of $M(\text{CH}_2)/M(\text{CF}_2) = 0.28$, meaning the spontaneous dissociation into $\text{CH}_2^+ + \text{CF}_2^+$ (or the counterpart of neutral radical) after Auger decays. The component with low kinetic energy indicates the second channel to produce the CH_2^+ and CF_2^+ fragment ions. The possibility is the excess energy relaxation into vibrational modes. That is, part of energy of the $\text{C}1s$ electron initially excited is redistributed into the CH , CCH and/or CCF vibrational modes with 0.4 eV spacing. This process competes with the direct dissociation of the $\text{C}=\text{C}$ chemical bond to form the main parts of the CF_2^+ and CH_2^+ ions. Thus, the second component lies in the low kinetic energy distribution with small anisotropy parameters: $\beta = -0.03$ and -0.16 for CF_2^+ and CH_2^+ , respectively, in the kinetic energy region less than 1 eV. From the present findings it is clear that molecular vibrations play an important role in the photofragmentation of K-shell excited molecule even in the small polyatomic molecule of CF_2CH_2 .

Summary

We have presented a brief review of the recent progress in the reaction dynamics of the K-shell excited polyatomic molecules. Kinetic energy distributions of fragment ions and site-specific photofragmentation after Auger decays are reasonably understood by the concept that intramolecular excess energy flows from the initially excited K-shell electron to vibrational modes of a polyatomic molecule. Some functional groups with vibrational modes in the molecule work as an effective energy reservoir or act as a barrier of energy flow. We believe that the present findings in the photofragmentation of the K-shell excited molecules are useful to understand the reaction dynamics for site-specific bond dissociation. In order to directly verify the photofragmentation which competes with intramolecular energy relaxation in a K-shell excited polyatomic molecule we need more sophisticated experiments in the near future.

Acknowledgements

The authors would like to thank all their co-workers for their fruitful cooperation [28, 30, 35, 38, 40, 44]. This work was supported by the joint program of the Institute for Molecular Science and was partly supported by a Grant-in-Aid for Scientific Research from the Ministry of Education, Culture, Sports, Science and Technology of Japan.

References

1. R.N. Zare, *Mol. Photochem.* 4 (1972) 1.
2. R.L. Dehmer, D. Dill, *Phys. Rev. A* 18 (1978) 164.
3. D. Dill, J.R. Swanson, S. Wallence, J.L. Dehmer, *Phys. Rev. Lett.* 45 (1980) 1393.
4. N. Saito, I.H. Suzuki, *Phys. Rev. Lett.* 61 (1988) 2740.
5. K. Lee, D.Y. Kim, C.I. Ma, D.A. Lopian-Smith, D.M. Hanson, *J. Chem. Phys.* 93 (1990) 7936.
6. A. Yagishita, E. Shigemasa, *Rev. Sci. Instrum.* 63 (1992) 1383.
7. N. Kosugi, E. Shigemasa, A. Yagishita, *Chem. Phys. Lett.* 190 (1992) 481.
8. N. Saito, I.H. Suzuki, *Phys. Rev. A* 43 (1991) 3662.
9. N. Kosugi, J. Adachi, E. Shigemasa, A. Yagishita, *J. Chem. Phys.* 97 (1992) 8842.
10. J.D. Bozek, N. Saito, I.H. Suzuki, *J. Chem. Phys.* 100 (1994) 393.
11. J.D. Bozek, N. Saito, I.H. Suzuki, *J. Chem. Phys.* 98 (1993) 4652.
12. J. Adachi, N. Kosugi, E. Shigemasa, A. Yagishita, *J. Chem. Phys.* 102 (1995) 7369.
13. J.D. Bozek, N. Saito, I.H. Suzuki, *Phys. Rev. A* 51 (1995) 4563.
14. J. Adachi, N. Kosugi, E. Shigemasa, A. Yagishita, *J. Chem. Phys.* 107 (1997) 4919.
15. N. Saito, K. Ueda, M. Simon, K. Okada, Y. Shimizu, H. Chiba, Y. Senba, H. Okumura, H. Ohashi, Y. Tamenori, S. Nagaoka, A. Hiraya, H. Yoshida, E. Ishiguro, T. Ibuki, I.H. Suzuki, I. Koyano, *Phys. Rev. A* 62 (2000) 042503.
16. D.Y. Kim, K. Lee, C.I. Ma, M. Mahalingam, D.M. Hanson, *J. Chem. Phys.* 97 (1992) 5915.
17. K. Okada, K. Ueda, T. Tokushima, Y. Senba, H. Yoshida, Y. Shimizu, M. Simon, H. Chiba, H. Okumura, Y. Tamenori, H. Ohashi, N. Saito, S. Nagaoka, I.H. Suzuki, E. Ishiguro, I. Koyano, T. Ibuki, A. Hiraya, *Chem. Phys. Lett.* 326 (2000) 314.
18. W. Eberhardt, T.K. Sham, R. Carr, S. Krumnacher, M. Strongin, S.L. Weng, D. Wesner, *Phys. Rev. Lett.* 50 (1983) 1038.
19. J. Murakami, M.C. Nelson, S.L. Anderson, D.M. Hanson, *J. Chem. Phys.* 85 (1986) 5755.
20. T. Gejo, K. Okada, T. Ibuki, N. Saito, *J. Phys. Chem.* 103 (1999) 4598.
21. W. Habenicht, H. Baiter, K. Müller-Dethlefs, E. W. Schlag, *J. Phys. Chem.* 95 (1991) 6774.
22. K. Müller-Dethlefs, M. Sander, L.A. Chewter, E.W. Schlag, *J. Phys. Chem.* 88 (1984) 6098.

23. S. Nagaoka, I. Koyano, K. Ueda, E. Shigemasa, Y. Sato, A. Yagishita, T. Nagata, T. Hayaishi, *Chem. Phys. Lett.* 154 (1989) 363.
24. I.H. Suzuki, N. Saito, J.D. Bozek, *Bull. Chem. Soc. Jpn.* 68 (1995) 1119.
25. I.H. Suzuki, N. Saito, *Int. J. Mass Spectrom. Ion Processes* 163 (1997) 229.
26. I.H. Suzuki, N. Saito, J.D. Bozek, *J. Electron Spectrosc. Relat. Phenom.* 101-103 (1999) 69.
27. M.K. Thomas, P.A. Hatherly, K. Codling, M. Stankiewicz, J. Rius, A. Karawajczyk, M. Roper, *J. Phys. B* 31 (1998) 3407.
28. T. Ibuki, K. Okada, T. Gejo, K. Saito, *J. Electron Spectrosc. Relat. Phenom.* 101-103 (1999) 149.
29. T. Ibuki, K. Okada, K. Saito, T. Gejo, *J. Electron Spectrosc. Relat. Phenom.* 107 (2000) 39.
30. K. Okada, S. Tanimoto, T. Morita, K. Saito, T. Ibuki, T. Gejo, *J. Phys. Chem. A* 107 (2003) 8444.
31. A. Hiraya, E. Nakamura, M. Hasumoto, T. Kinoshita, K. Sakai, E. Ishiguro, M. Watanabe, *Rev. Sci. Instrum.* 66 (1995) 2104.
32. R.N.S. Sodhi, C.E. Brion, *J. Electron Spectrosc. Relat. Phenom.* 34 (1984) 363.
33. J.A.R. Samson, *Techniques of Vacuum Ultraviolet Spectroscopy*, Wiley, New York, 1967.
34. W.C. Wiley, I.H. McLaren, *Rev. Sci. Instrum.* 26 (1955) 1150.
35. T. Ibuki, K. Okada, K. Saito, T. Gejo, N. Saito, I.H. Suzuki, *Nucl. Instrum. Methods Phys. Res. A* 467-468 (2001) 1505.
36. L. Claisen, *Ber. Dtsch. Chem. Ges. (Berlin)* 25 (1892) 1776.
37. Y. Kawasaki, A. Fujii, Y. Nakano, S. Sakaguchi, Y. Ishii, *J. Org. Chem.* 64 (1999) 4214.
38. T. Ibuki, K. Okada, S. Tanimoto, K. Saito, T. Gejo, *J. Electron Spectrosc. Relat. Phenom.* 123 (2002) 323.
39. K. Okada, S. Tanimoto, T. Ibuki, K. Saito, T. Gejo, *Chem. Lett. (Jpn.)* 2001 (2001) 1046.
40. T. Ibuki, K. Okada, T. Gejo, K. Saito, *Chem. Phys. Lett.* 328 (2000) 147.
41. A.P. Hitchcock, M. Tronc, A. Modelli, *J. Phys. Chem.* 93 (1989) 3068.
42. N. Saito, I.H. Suzuki, *Int. J. Mass Spectrom. Ion Processes* 82 (1988) 61.
43. T. Gejo, E. Nakamura, E. Shigemasa, *UVSOR Activity Report* 1999 (2000) 39.
44. K. Okada, S. Tanimoto, T. Ibuki, Y. Haga, T. Gejo, K. Saito, K. Ohno, *Chem. Phys.* submitted.
45. W.L. Jolly, K.D. Bomben, C.J. Eyermann, *At. Data Nucl. Data Tables* 31 (1984) 433.
46. R. McLaren, S.A.C. Clark, I. Ishii, A.P. Hitchcock, *Phys. Rev. A* 36 (1987) 1683.